Absorption effects in liquid crystal waveguides

J. A. Reyes and R. F. Rodríguez*
Departamento de Física Química, Instituto de Física, UNAM, Apartado Postal 20-364, 01000 México D.F., Mexico
(Received 30 May 2003; published 27 October 2003)

An analytical and numerical study of the propagation of optical fields through a nematic hybrid slab is developed. We take into account explicitly the absorption of radiation by the liquid crystal by introducing a complex dielectric tensor. For a low intensity beam we first derive the eikonal equation and from it we calculate the ray trajectories in the optical limit. We show that in the presence of absorption, there are no caustics within the slab. Then we consider the WKB limit and calculate the field transverse magnetic modes, their number and their cutoff frequencies. We show that for both limits the agreement between our analytical and numerical results for the propagation constants is excellent, while there are larger differences in the analytically and numerically calculated field amplitudes. These differences show that absorption effects are important for this quantity and have their origin in the fact that the chosen parameter values in our exact numerical calculations, strictly speaking, do not lie within the limits of validity of the WKB approximation. Although a more precise comparison between these approaches requires the use of different sets of values of the relevant parameters, our analysis shows the effects and complications arising from the inclusion of absorption. Finally, we discuss the scope and limitations of our approach.

DOI: 10.1103/PhysRevE.68.041707 PACS number(s): 42.65.Jx, 78.20.Jq, 78.20.Ci

I. INTRODUCTION

The huge optical response of liquid crystalline materials has made possible the production of gigantic optical nonlinearities [1] and strong nonlinear effects by using lasers with moderate intensity (kW/cm^2) [2]. This high sensitivity of liquid crystals (LCs) has allowed us to use them to control the light output of optical devices such as waveguides [3–6] or optical fibers [7,8].

The phenomenon of light-induced molecular reorientation is at the basis of the high nonlinear response of liquid crystals and has been a subject of intense research activity in the last decade [9,10]. However, in spite of these features which make their use so attractive in the design of optical devices, liquid crystals also show important limitations which might be related to the characteristics of light absorption in these systems. Some of them are, for instance, their slow response times (milliseconds) or the strong absorption and scattering losses ($20\ dB\ cm^{-1}$) they exhibit [11]. These effects due to absorption are greatly enhanced when small traces of light absorbing molecules (less than 1%) are added to the system. Their presence can strongly alter the character of their interaction with light and may reduce the threshold intensity for the optical Freedericksz transition by two orders of magnitude, giving rise to the so called Jánossy effect [12–14].

In recent works different nonlinear optical phenomena in dye-doped LC waveguides have been studied theoretically and experimentally. These include the nonlinear beam splitting activated above certain light intensity threshold [15], the nonlinear mode coupling mismatch between the sections of a three-section guiding device and the decreasing output power versus increasing input power [16]. Although LC optical devices are carefully designed to work in the wavelength range for which the absorption effect is practically negligible, here we are interested in studying those ranges where this effect is noticeable. Particularly, we shall analyze this effect for dye-doped nematics that have been experimentally shown to have a wavelength range around the dye color where absorption is considerable [17,18].

More specifically, in this work the propagation of an electromagnetic wave through an absorbing doped, hybrid, planar, nematic cell is studied analytically and numerically. The absorption effects in the propagation of radiation through a nematic are taken into account by assuming a complex nematic dielectric tensor, whose imaginary part is due to the absorbing dye doping. However, the strong orientational nonlinearity is not considered and the nematic's orientation is assumed to remain constant, that is, our analysis is restricted to analyze the linear propagation regime. We generalize a previously developed formalism [6–8] to include the propagation of optical fields in absorbing media. This generalization consists of performing a systematic analysis in power of the dimensionless parameter $k_0 l$, which measures the ratio between the thickness slab l and the wavelength of the optical field. By varying $k_0 l$ from very large values to values of the order of 10, the electromagnetic fields are suitable to be described by rays or quasiplanar waves corresponding, respectively, to the so called optical limit (OL) and the WKB limit. In the OL we find and solve a complex eikonal equation and calculate the ray trajectories, whereas for the WKB approximation we obtain the field amplitudes. We discuss a generalization of Fermat's principle for a lossy, anisotropic inhomogeneous medium and give an interpretation of the complex ray trajectories. By using experimental values for the refractive indices of the doped nematic, we compare our analytical and numerical results for the propagation constant with absorption, with previously derived analytical and numerical results without absorption [19]. This comparison shows that absorption effects for this model calculation may be quite large for some properties and play an important role in this propagation process. More specifically, for the propa-

*Corresponding author. Email address: zepeda@fisica.unam.mx

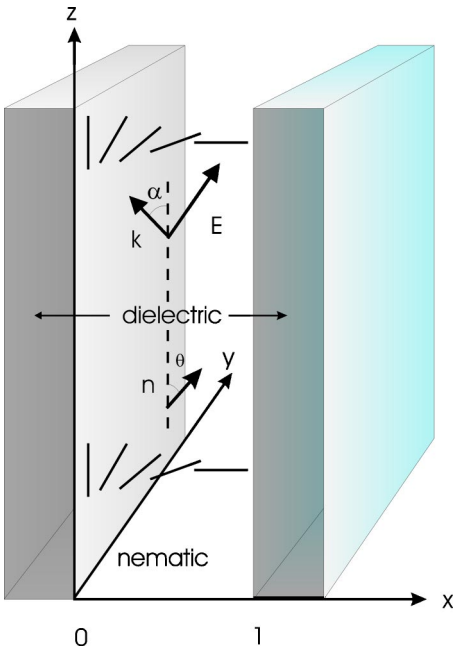

FIG. 1. Schematics of a hybrid slab waveguide.

gation constant with and without absorption, we get an excellent agreement, which indicates that for this property absorption effects are small. In contrast, a comparison of the field amplitudes for the absorption and absorptionless situations, show that absorption effects may be quite large and should be taken into account in the dynamic description.

II. MODEL AND BASIC EQUATIONS

Consider a dye-doped nematic crystal layer of thickness l contained between two parallel isotropic dielectric media, as shown in Fig. 1. The transverse dimensions along the x and y directions are large compared to l, but the cell has a finite volume $V=L\ l$. In the absence of external optical fields, the nematic will retain its initial orientation $\hat{n}$. However, if it is excited by an obliquely applied laser beam in the x-z plane, the orientation of the director inside the cell will change with position and time. If the polarization of the beam always remains in the plane of incidence, in the absence of backflows the reorientation of $\hat{n}$ will also take place in the x-z plane and

$$\hat{n}=(\sin\theta(x,t),0,\cos\theta(x,t)), \tag{1}$$

where θ is the reorientation angle defined with respect to the z axis in Fig. 1. An initially hybrid configuration of the director field which is parallel to the boundary at $x=0$ and perpendicular to it on $x=1$ is assumed. The corresponding boundary conditions on θ are then

$$\theta(x=0)=0, \quad \theta(x=1)=\pi/2. \tag{2}$$

In previous works we have described the propagation of electromagnetic waves within planar and cylindrical nematic cells in terms of the dynamics of the complete representation provided by the transverse magnetic (TM) modes, $E_x(x,k_0)$, $E_z(x,k_0)$, and $H_y(x,k_0)$, where $k_0=\omega/c$ is the free space wave number, ω the frequency of the field, and c the speed of light in vacuum [6,23,24]. These modes are the only ones that couple to the reorientational dynamics of $\hat{n}$. As will be seen below, the inclusion of absorption of the incident optical field by the dye-doped nematic liquid crystal preserves this description in terms of TM modes. For this purpose we use the same constitutive relation

$$D_i=\epsilon_{ij}E_j, \tag{3}$$

but with a uniaxial dielectric tensor $\epsilon_{ij}=\epsilon_\perp\delta_{ij}+\epsilon_a n_i n_j$, which is now a complex quantity. This means that the dielectric constants perpendicular and parallel to the long axis of the molecules, namely, $\epsilon_\perp\equiv\epsilon_\perp^r+i\epsilon_\perp^i$ and $\epsilon_\parallel\equiv\epsilon_\parallel^r+i\epsilon_\parallel^i$, are also complex numbers whose imaginary parts describe the absorption of the dyed nematic. The dielectric anisotropy is $\epsilon_a\equiv\epsilon_\parallel-\epsilon_\perp$ and, as usual, $i\equiv\sqrt{-1}$ denotes the imaginary unit. In terms of the dimensionless variable $\zeta\equiv x/l$ and for the geometry in Fig. 1, the components of ϵ_{ij} are the following explicit functions of θ, $\epsilon_{zz}=\epsilon_\perp+\epsilon_a\cos^2\theta(\zeta)$, $\epsilon_{xx}=\epsilon_\perp+\epsilon_a\sin^2\theta(\zeta)$, and $\epsilon_{xz}=\epsilon_a\sin\theta(\zeta)\cos\theta(\zeta)$.

As for the case without absorption, we use Maxwell's equations without sources to describe the optical field within the liquid crystal [24] and we arrive at the following general set of equations for the amplitudes of the TM modes, uncoupled to the corresponding transverse electric (TE) modes, namely,

$$\epsilon_{zz}\frac{d^2H_y}{d\zeta^2}+\left[2ik_0lp\epsilon_{xz}+\frac{d\epsilon_{zz}}{d\zeta}\right]\frac{dH_y}{d\zeta}$$
$$+k_0l\left[k_0l(\epsilon_\parallel\epsilon_\perp-p^2\epsilon_{zz})+ip\frac{d\epsilon_{zz}}{dz}\right]H_y=0, \tag{4}$$

$$E_z=\frac{1}{\epsilon_\parallel\epsilon_\perp}\left\{-\epsilon_{xx}pH_y+\frac{i}{k_0l}\epsilon_{xz}\frac{dH_y}{d\zeta}\right\}, \tag{5}$$

$$E_x=\frac{1}{\epsilon_\parallel\epsilon_\perp}\left\{p\epsilon_{zz}H_y-\frac{i}{k_0l}\epsilon_{xz}\frac{dH_y}{d\zeta}\right\}. \tag{6}$$

Here $p\equiv\beta/k_0$, where β denotes the propagation constant of the mode and $\zeta\equiv x/l$. As a consequence of the complex character of ϵ_{ij}, β is also a complex quantity, $\beta=\beta^r+i\beta^i$. Its real part β^r describes the propagation of the optical field along the waveguide and its imaginary part β^i is inversely proportional to the penetration length due to absorption effects.

As usual, the stationary orientational configurations are determined by minimizing the Helmholtz free energy functional of the model [6,19]. In this work we shall only consider the final stationary orientational state after reorientation has occurred. This state is defined by the corresponding Euler-Lagrange equation, which in dimensionless form reads

$$\frac{d^2\theta}{d\zeta^2}+q[\sin 2\theta(|\overline{E}_x|^2-|\overline{E}_z|^2)+(\overline{E}_x\overline{E}_z^*+\overline{E}_z\overline{E}_x^*)\cos 2\theta]=0. \tag{7}$$

Here $\bar{E}_x \equiv E_x/E_0$, $\bar{E}_z \equiv E_z/E_0$, and $I \equiv cE_0^2/8\pi$ is the intensity of the incident field; * indicates complex conjugate. The parameter $q \equiv cE^2 l^2/8\pi K$, where K is the elastic constant in the equal constant approximation, is proportional to the ratio between the electric energy of the beam to the elastic energy of the nematic and, therefore, measures the strength of the coupling between the optical field and the orientational configuration of the nematic. Clearly, to close the orientational equation (7) it is necessary to determine first the TM modes. Although this may be accomplished to different orders of approximation in the parameter $k_0 l$, here we only consider the OL and the WKB limit which are defined, respectively, by the conditions $k_0 l \gg 1$ and $k_0 l > 1$ [25]. For the OL we can neglect the wavelike behavior of the optical field and to describe it, it is enough to consider the locus traced by the field amplitude maximum, which is referred to as the ray trajectory, On the other hand, for the WKB limit in which $k_0 l$ is not so large, not only the phase of the wave has spatial variations but the field amplitude as well.

III. OPTICAL FIELD DYNAMICS

Now, since the concept of ray trajectory is defined only in the OL, and the TM modes will be required in the WKB limit later on, following the usual procedure of geometrical optics, we assume that the TM modes may be written in the form

$$E_j(\vec{r},t) = E_{0j}(\vec{r}) \exp[i\{k_0 l W(\vec{r}) - \omega t\}], \quad j = x,z, \tag{8}$$

$$H_y(\vec{r},t) = H_{0y}(\vec{r}) \exp[i\{k_0 l W(\vec{r}) - \omega t\}], \tag{9}$$

where the Hamilton's characteristic function W is now a complex quantity, $W = W^r + iW^i$. This generalizes the idea of optical path in such a way that its real part W^r describes the usual optical path between two fixed points of a medium, whereas its imaginary component W^i measures the absorption of the electromagnetic wave when it propagates through the liquid crystal. If Eqs. (8) and (9) are substituted into Eqs. (4)–(6) and the resulting equations are solved up to terms of order zero and one in the parameter $(k_0 l)^{-1}$, we arrive at the following eikonal equation:

$$\epsilon_{xx}\left(\frac{\partial W}{\partial \chi}\right)^2 + \epsilon_{zz}\left(\frac{\partial W}{\partial \zeta}\right)^2 + 2\epsilon_{xz}\left(\frac{\partial W}{\partial \chi}\right)\left(\frac{\partial W}{\partial \zeta}\right) = \epsilon_\parallel \epsilon_\perp , \tag{10}$$

with $\chi \equiv z/l$. As for the case where W is real, we solve this equation by using the following canonical transformation:

$$W(\zeta,\chi) = p\chi + S(\zeta), \tag{11}$$

but where W, p, and $S(\zeta)$ are all complex quantities. Substitution of Eq. (11) into Eq. (10) yields the following ordinary differential equation for $S(\zeta)$:

$$\epsilon_{zz}\left[\frac{dS(\zeta)}{d\zeta}\right]^2 + 2p\epsilon_{xz}\frac{dS(\zeta)}{d\zeta} + p^2\epsilon_{xx} - \epsilon_\parallel\epsilon_\perp = 0, \tag{12}$$

whose general solution for a given initial condition S_0 reads

$$S_\pm(\zeta) = \int_0^\zeta d\zeta' \frac{-p\epsilon_{zx} \pm [\epsilon_\parallel \epsilon_\perp (\epsilon_{zz} - p^2)]^{1/2}}{\epsilon_{zz}} + S_0 . \tag{13}$$

Thus, from Eq. (11) we arrive at

$$W(\zeta,\chi) = p\chi + \int_0^\zeta d\zeta' \frac{-p\epsilon_{zx} \pm [\epsilon_\parallel \epsilon_\perp (\epsilon_{zz} - p^2)]^{1/2}}{\epsilon_{zz}} + S_0 . \tag{14}$$

By using the general theory of the Hamilton-Jacobi equation [26], we derive the following equation for the ray trajectories:

$$\gamma = \chi - \int_0^\zeta d\eta \left[\frac{\epsilon_{xz}}{\epsilon_{zz}} + \frac{p}{\epsilon_{zz}}\sqrt{\frac{\epsilon_\perp \epsilon_\parallel}{\epsilon_{zz} - p^2}}\right], \tag{15}$$

where γ is the invariant generalized coordinate conjugated to p. It should be stressed that χ is also complex, $\chi = \chi_r + i\chi_i$. As usual, its real part χ_r gives the path along which the intensity of the field is maximum, that is, it defines the ray trajectory. However, it is modified by the imaginary part χ_i, which represents the path along which dissipation is a minimum, as will be shown in the following section. In this sense, it defines a dissipation function depending on ζ. Furthermore, in contrast to the absorptionless case [7], here it is not obvious that there is a singularity in the trajectory (caustic) when $\epsilon_{zz} = p^2$, as suggested by Eq. (15), because this condition is now complex. Actually, it will be shown below for a specific dyed-doped nematic that indeed there are no caustics when absorption is present.

The propagation constant p may be expressed in terms of the propagation angle α, defined in Fig. 1, by evaluating $d\chi/d\zeta$ at $\zeta = 0$ from Eq. (15). This leads to

$$p = \bar{\epsilon} \frac{\tan\alpha - \dfrac{\epsilon_a}{2}}{\sqrt{\left(\tan\alpha - \dfrac{\epsilon_a}{2}\right)^2 + \dfrac{\epsilon_\perp \epsilon_\parallel}{\bar{\epsilon}}}}, \tag{16}$$

where $\bar{\epsilon} \equiv (\epsilon_\perp + \epsilon_\parallel)/2$. However, to calculate the trajectory explicitly, it is necessary to know the functions $\epsilon_{ij}(\theta)$. In this work we shall only consider the case in which the dynamics of the field is completely decoupled to the orientational dynamics, i.e., $q = 0$. Then, from Eq. (7) the stationary configurational state turns out to be

$$\theta = \frac{\pi}{2}\zeta. \tag{17}$$

With this result the components of ϵ_{ij} in Eq. (15) can be determined as explicit functions of ζ. To calculate the real and imaginary parts of two ray trajectories for two incidence angles, we take the material parameters of the nematic phase of ZhKM−1277 with small additions (1 wt %) of dye I [17]. This substance possesses a nematic phase in the temperature range $-20\,^\circ\mathrm{C} < T < 60\,^\circ\mathrm{C}$ and it is characterized by a positive low-frequency dielectric anisotropy $\Delta\epsilon = 12.2$. Dye I ex-

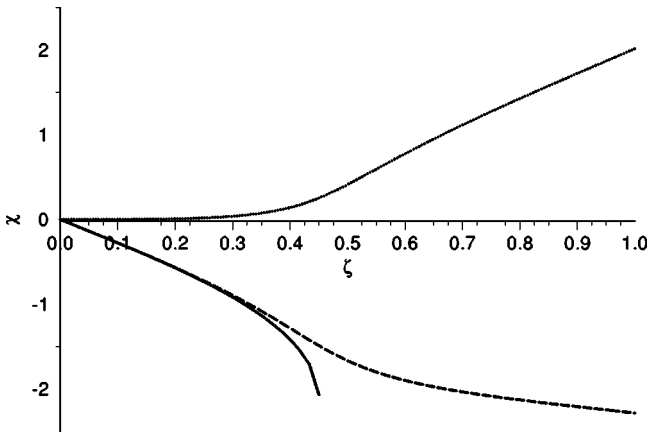

FIG. 2. Real (- - -) and imaginary ($\cdot\ \cdot\ \cdot$) parts of the ray trajectory for $\alpha=40°$ for the nematic phase of doped ZhKM -1277. (—) denotes the case without absorption.

hibits positive dichroism. From their measurements of the polarization absorption spectra of the dyes as a function of the wavelength of the light (see Fig. 1 in Ref. [17]), for a concentration $\sim 1\%$ and $\lambda \sim 640$ nm, one gets that $\epsilon_\perp = 2.25 + i1.0$, $\epsilon_a = 0.64 + i0.02$. Inserting these values into Eq. (15), we plot the real and imaginary parts of the trajectory for $\alpha=40°$ and $\alpha=70°$, respectively, as shown in Figs. 2 and 3. We have included as a reference the trajectory for the absorptionless case, as calculated in Ref. [24]. These plots show that, indeed, there are no caustics even in the absorptionless limit, which corresponds to what we have denoted as the weak limit in Ref. [24]. The dissipation function χ_i increases continuously as the ray moves towards the right hand side end of the cell and χ_r is less deflected than the trajectory without absorption. On the other hand, $\alpha=70°$ corresponds to the strong regime limit [24], which exhibits a caustic at $\zeta_c=0.48$ when absorption is absent. The trajectory is always real for $\zeta<\zeta_c$ and as a consequence, the field amplitude oscillates. In contrast, for $\zeta>\zeta_c$ the trajectory is no longer defined and the field amplitude is evanescent. Moreover, the dissipation function χ_i increases at a notoriously larger rate precisely at $\zeta=\zeta_c$, indicating that the amplitude of the propagating field will decrease for $\zeta>\zeta_c$. Thus, the field's energy is more concentrated in the region $\zeta<\zeta_c$ even

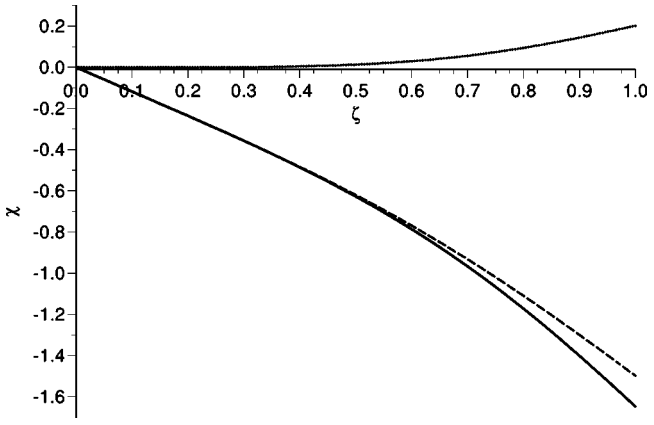

FIG. 3. The same as in Fig. 2 for $\alpha=70°$.

though χ_i is small and a description which totally neglects absorption [20–22,7,27] is expected to be valid in this region; but absorption effects cannot be ignored for $\zeta>\zeta_c$.

IV. TM MODES

Consider now the TM modes. According to Eq. (8), the phase of the TM modes is determined in the OL. However, to calculate the amplitudes $E_{0j}(\vec{r})$, $H_{0y}(\vec{r})$ as a function of position within the cell, it is necessary to solve Eqs. (4)–(6) in the WKB limit, since in the OL the field amplitudes are constant. For this purpose we assume that

$$S(\zeta)=S_{\pm}^{(0)}(\zeta)+S^{(1)}(\zeta), \tag{18}$$

where the superscript denotes the solutions of Eq. (12) up to vanishing and first order in $(k_0 l)^{-1}$. Substitution of this form of $S(\zeta)$ into Eq. (12) leads to

$$\frac{dS^{(1)}(\zeta)}{d\zeta}=\pm\frac{i}{2k_0 l}\frac{\epsilon_{zz}\dfrac{d^2S_{\pm}^{(0)}}{d\zeta^2}+\dfrac{d\epsilon_{zz}}{d\zeta}\dfrac{dS_{\pm}^{(0)}}{d\zeta}+p\dfrac{d\epsilon_{xz}}{d\zeta}}{\sqrt{\epsilon_\parallel\epsilon_\perp(\epsilon_{zz}-p^2)}}, \tag{19}$$

whose general solution is

$$S(\zeta)=S_{\pm}^{(0)}(\zeta)+\frac{i}{2k_0 l}\ln\sqrt{\epsilon_\parallel\epsilon_\perp(\epsilon_{zz}-p^2)}+C_\pm. \tag{20}$$

Here $C_\pm$ are integration constants that will be determined from the boundary conditions for the TM modes. For a given k_0, these conditions take the form [28]

$$H_y^L|_{\zeta=0}=H_y|_{\zeta=0}, \tag{21}$$

$$\frac{1}{\epsilon_c}\frac{dH_y^L}{dy}\bigg|_{\zeta=0}=\frac{1}{\epsilon_\parallel}\frac{dH_y}{dy}\bigg|_{\zeta=0}, \tag{22}$$

$$H_y^R|_{\zeta=1}=H_y|_{\zeta=1}, \tag{23}$$

$$\frac{1}{\epsilon_c}\frac{dH_y^R}{dy}\bigg|_{\zeta=1}=\frac{1}{\epsilon_\perp}\frac{dH_y}{dy}\bigg|_{\zeta=1}. \tag{24}$$

The superscripts L and R identify the isotropic dielectric media to the left and right of the nematic layer and ϵ_c denotes the dielectric constant of the isotropic cladding.

Substitution of Eq. (20) into Eq. (9) yields the two independent solutions for $H_y(\zeta,t)$ and their linear combination gives the general solution

$$H_y(\zeta,k_0)=\left[\frac{\epsilon_\perp\epsilon_\parallel}{(\epsilon-p^2)}\right]^{1/4}e^{i\phi(\zeta,k_0)}\left[C\cos\left(k_0 l\int_0^\zeta f(\eta,k_0)d\eta\right)+D\sin\left(k_0 l\int_0^\zeta f(\eta,k_0)d\eta\right)\right], \tag{25}$$

where C and D are two arbitrary constants to be determined also from the above boundary conditions. The functions ϕ and $f(\eta,k_0)$ are defined, respectively, by

$$\phi(\zeta,k_0)\equiv -ipk_0l\int_0^{\zeta}d\eta\frac{\epsilon_{xz}}{\epsilon_{zz}} \tag{26}$$

and

$$f(\eta,k_0)\equiv\frac{\sqrt{\epsilon_{\perp}\epsilon_{\parallel}(\epsilon_{zz}-p^2)}}{\epsilon_{zz}}. \tag{27}$$

On the other hand, it is well known that $H_y(\zeta,k_0)$ in the isotropic dielectric claddings without absorption is governed by the following equation [29]:

$$\frac{d^2H_y}{d\zeta^2}+(k_0l)^2(\epsilon_c-p^2)H_y=0. \tag{28}$$

Solutions of Eq. (28) which vanish at infinity for the left, H_y^L, and right, H_y^R, dielectric claddings are given by

$$H_y^L=Fe^{k_0l\sqrt{p^2-\epsilon_c}\zeta}, \tag{29}$$

$$H_y^R=Ge^{-k_0l\sqrt{p^2-\epsilon_c}\zeta}, \tag{30}$$

where G and F are also undetermined constants. To find the four constants C, D, G, and F, it is necessary to impose the boundary conditions (21)–(24). If we insert Eqs. (25), (29), and (30) into these boundary conditions, place the origin of the reference system at the left boundary of the slab, and solve the resulting system of equations, we arrive at the following expressions for the TM modes in terms of p or α for the different regions of the cell:

$$H_y^L(\zeta,k_0)=\frac{\epsilon_c}{\sqrt{p^2-\epsilon_c}}\sqrt[4]{\frac{\epsilon_{\parallel}-p^2}{\epsilon_{\parallel}\epsilon_{\perp}}}e^{k_0l\sqrt{p^2-\epsilon_c}\zeta}, \tag{31}$$

$$H_y(\zeta,k_0)=\frac{e^{i\phi(\zeta,k_0)}}{\sqrt[4]{\epsilon_{\perp}\epsilon_{\parallel}(\epsilon_{xx}-p_n^2)}}\left[\sin\left(k_0l\int_0^{\zeta}d\eta f(\eta,k_0)\right)+\epsilon_c\sqrt{\frac{\epsilon_{\parallel}-p^2}{\epsilon_{\perp}\epsilon_{\parallel}(p^2-\epsilon_c)}}\cos\left(k_0l\int_0^{\zeta}d\eta f(\eta,k_0)\right)\right], \tag{32}$$

$$H_{yn}^R=\frac{D}{\sqrt[4]{\epsilon_{\parallel}\epsilon_{\perp}(\epsilon_{\parallel}-p_n^2)}}e^{\phi_c+\sqrt{p_n^2-\epsilon_c}k_0l(1-\zeta)}\times\left[\sin\phi_c+\epsilon_c\sqrt{\frac{\epsilon_{\perp}-p_n^2}{\epsilon_{\parallel}\epsilon_{\perp}(p_n^2-\epsilon_c)}}\cos\phi_c\right], \tag{33}$$

where $\phi_c\equiv k_0l\int_0^1 d\eta f(\eta,k_0)$. The remaining TM mode components $E_x(z,k_0)$ and $E_z(z,k_0)$ are obtained from Eqs. (6) and (5), respectively. However, not all the values of α generate a propagation TM mode. The discrete values that do so will be denoted by p_n, where the subindex n identifies the corresponding mode. From Eqs. (25), (29), and (30), it follows that the allowed values of p_n are given by the solution of the complex transcendental equation

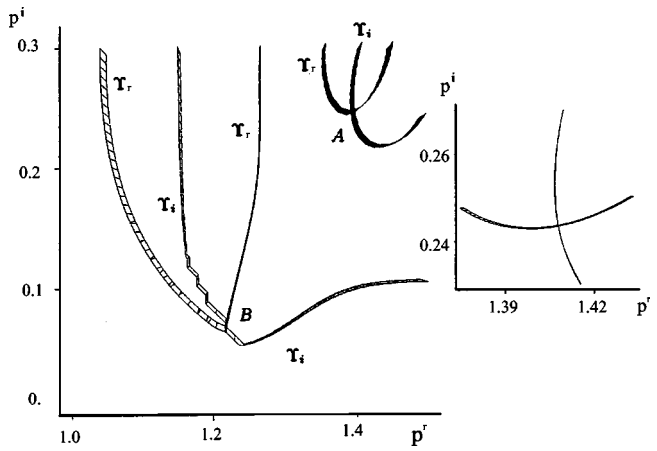

FIG. 4. Graphic solution of the trascendental equation (34) as a function of the propagation constant $p=p^r+ip^i$ for the range $(-0.001,0.001)$ for Υ_r and Υ_i, and for the intervals $1\leqslant p^r\leqslant 1.5$ and $0\leqslant p^i\leqslant 0.3$. The inset shows in more detail solution A for the mode $n=1$.

$$\sqrt{\frac{\epsilon_{\parallel}\epsilon_{\perp}(p_n^2-\epsilon_c)}{\epsilon_{\parallel}-p_n^2}}-\frac{\tan\phi_c+\sqrt{\dfrac{\epsilon_{\parallel}\epsilon_{\perp}(p_n^2-\epsilon_c)}{\epsilon_{\perp}-p_n^2}}}{1-\tan\phi_c\sqrt{\dfrac{\epsilon_{\parallel}\epsilon_{\perp}(p_n^2-\epsilon_c)}{\epsilon_{\perp}-p_n^2}}}\equiv\Upsilon_r+i\Upsilon_i=0. \tag{34}$$

The real and imaginary parts of the difference between the right and left hand sides of Eq. (34) are plotted in Fig. 4 as functions of the parameter $p_n=p_n^r+ip_n^i$, for the same material parameters used in Fig. 2. Note that both Υ_r and Υ_i are surfaces in the complex plane and the roots of Eq. (34) are determined by the intersection of these surfaces. For this reason in Fig. 4 only those sections of these surfaces that lie in the range $(-0.001,0.001)$ are plotted as functions of p^r and p^i in the intervals $1\leqslant p^r\leqslant 1.5$ and $0\leqslant p^i\leqslant 0.3$, respectively. Although their intersection appears as an extended area in Fig. 4, it is always possible to reduce this area to a single point, which represents the solution of Eq. (34). This is shown in the inset of Fig. 4. Actually, only two of the several possible solutions, A and B, are shown; they correspond, respectively, to the lowest order modes $n=1,2$. The eigenvalue corresponding to A, $\sigma^{n=1}$, is given by the coordinates of the point $(p_{n=1}^r=1.403,\ p_{n=1}^i=0.243)$, namely, $p_A=1.403+i0.243$, see inset in Fig. 4. Similarly, the eigenvalue associated with B is $p_B=1.1892+i0.575$.

Let us now derive an expression for the cutoff frequency ω_{c_n} for the TM mode of order n. This is accomplished by setting $p_n^2=\epsilon_c$ in Eq. (34). Since ϵ_c is real, this condition yields the minimum value of p_n in order to have a propagating TM mode in the slab. Then, from Eq. (34) we get

$$\omega_{c_n} = \frac{nc\pi}{l}\frac{1}{\Delta}, \tag{35}$$

with

$$\frac{1}{\Delta} \equiv \frac{2}{\pi}\sqrt{\frac{\epsilon_\parallel \epsilon_\perp}{\epsilon_\parallel - \epsilon_c}}\left[K\left(\frac{\epsilon_a}{\epsilon_\parallel - \epsilon_c}\right) - \frac{\epsilon_c}{\epsilon_\parallel}\Pi\left(\frac{\epsilon_a}{\epsilon_\parallel}, \frac{\epsilon_a}{\epsilon_\parallel - \epsilon_c}\right)\right], \tag{36}$$

and where K and Π denote the complete elliptic functions of first and third classes, respectively. For the nematic phase of doped ZhKM−1277 we get $\Delta = 0.852 + i0.602$. Upon substitution into Eq. (35) we get for $n=1$ and $l=10^{-5}$ m, $\mathrm{Re}[\omega_{c_n}] = 7.346\times 10^{13}$ Hz and $\mathrm{Im}[\omega_{c_n}] = -5.201 \times 10^{13}$ Hz. As usual, $\mathrm{Re}[\omega_{c_n}]$ gives the minimum frequency for which the mode propagates. On the other hand, note that when $\mathrm{Im}[\omega_{c_n}]$ is inserted into Eqs. (8) and (9) the field has a damped contribution. Therefore, $\mathrm{Im}[\omega_{c_n}]$ denotes the minimum frequency of a damped wave that remains inside the waveguide.

V. GENERALIZED FERMAT'S PRINCIPLE

To justify the interpretation of the complex ray trajectories used in the last section, here we discuss the generalization of Fermat's principle for an anisotropic inhomogeneous medium. Recall that Fermat's principle for an isotropic nonabsorbing medium, establishes that the trajectory traced by a ray between two fixed points of the medium is such that the optical path $l = \int_{P_1}^{P_2}\sqrt{\epsilon}ds$, where ϵ is the dielectric constant of the medium and s is the arc length of the trajectory, is minimized. To extend this principle to the case of a general lossy, anisotropic inhomogeneous medium we follow the procedure introduced by Born and Wolf [30]. Consider a tensor $\epsilon_{ij}(\vec{r})$ depending on the dielectric tensor and note that the only scalar proportional to $\epsilon_{ij}(\vec{r})$ and quadratic in dx_i which can be constructed is $\epsilon_{ij}dx_i dx_j$. Thus, we propose the following generalization for the optical path $U(\vec{r}, d\vec{r}/d\tau)$;

$$U\left(\vec{r}, \frac{d\vec{r}}{d\tau}\right) = \int_{P_1}^{P_2} d\tau \sqrt{\epsilon_{ij}\frac{dx_i}{d\tau}\frac{dx_j}{d\tau}}, \tag{37}$$

where τ is an arbitrary but monotonous parameter. If $U(\vec{r}, d\vec{r}/d\tau)$ is now minimized by applying the Euler-Lagrange equations we arrive at the expression

$$0 = \frac{\delta U}{\delta x_k} = \frac{d}{d\tau}\frac{\epsilon_k \dfrac{dx_i}{d\tau}}{\sqrt{\epsilon_{jm}\dfrac{dx_j}{d\tau}\dfrac{dx_m}{d\tau}}} - \frac{dx_s}{d\tau}\frac{dx_n}{d\tau}\frac{\partial}{\partial x_k}\frac{\epsilon_{sn}}{\sqrt{\epsilon_{jm}\dfrac{dx_j}{d\tau}\dfrac{dx_m}{d\tau}}}, \tag{38}$$

which allows us to determine parametrically the ray trajectories. From this equation the Hamiltonian variables known as the ray components are given by

$$p_j = \frac{\epsilon_{ij}\dfrac{dx_i}{d\tau}}{\sqrt{\epsilon_{km}\dfrac{dx_k}{d\tau}\dfrac{dx_m}{d\tau}}}, \tag{39}$$

and from here the invariant $p_j dx_j/d\tau$ equals the Lagrangian, Eq. (37). Thus, Eq. (39) leads exactly to

$$p_i \epsilon_{ij}^{-1} p_j = 1 \tag{40}$$

and proves that Eq. (37) is, indeed, a Lagrangian density or extended optical path. It is interesting to note that this ''extended'' Fermat's principle is similar to the variational principle for geodesics in gravitation [31], where in this case $\epsilon_{ij}(\vec{r})$ plays the role of the metric tensor $g_{ij} = -\epsilon_{ij}(\vec{r})$. In this sense the optical trajectory is equivalent to a beam moving through a curved space imposed by the dielectric tensor. This type of analogies have been used recently for analyzing the behavior of anisotropic nonabsorbing media [32].

So far, it has not been proven that the extremals of U are indeed minima. We shall now state the Weiestrass' and Legendre's conditions necessary for a real minimum. Let $\overline{x}(\tau)$, $\overline{y}(\tau)$, and $\overline{z}(\tau)$ be a fixed extremal $\overline{C}$ embedded in a field u, v, w, and let $x(\tau)$, $y(\tau)$, and $z(\tau)$ be any neighboring curve C also embedded in the field with the same end points P_1 and P_2 as $\overline{C}$. Then, the extremum will be a real minima if

$$\int_C U(x',y',z',x,y,z)d\tau - \int_{\overline{C}} U(\overline{x'},\overline{y'},\overline{z'},\overline{x},\overline{y},\overline{z})d\tau > 0. \tag{41}$$

Using the Hilbert's independence integral [33], we may replace the second integral by one extended not over $\overline{C}$ but over C. This yields

$$\int_C U d\tau - \int_{\overline{C}} U d\tau = \int \mathcal{E}(\overline{x'},\overline{y'},\overline{z'},\overline{x},\overline{y},\overline{z})d\tau > 0, \tag{42}$$

where

$$\begin{aligned}\mathcal{E}(\overline{x'},\overline{y'},\overline{z'},\overline{x},\overline{y},\overline{z},u_1,u_2,u_3) &= U(x',y',z',x,y,z) - U(u_1,u_2,u_3,x,y,z) \\ &\quad - (x_i' - u_i)U_{u_i}(u_1,u_2,u_3,x,y,z).\end{aligned} \tag{43}$$

This function is called the excess function of Weiestrass [34]. It is seen that $\mathcal{E}$ vanishes on any portion of C which coincides with a field extremal. Then we construct a special curve C such that between P_1 and a point A, the curve coincides with a field extremal. From A to a point B on the given extremal, it is a straight line, and from B to P_2, it coincides with the given extremal. Then $\mathcal{E}$ vanishes on the parts P_1A and BP_2, but

$$\int_A^B \mathcal{E} d\tau > 0. \tag{44}$$

By letting A approach B, its is seen that this inequality is only possible if

$$\mathcal{E}(\overline{x'},\overline{y'},\overline{z'},\overline{x},\overline{y},\overline{z}) > 0, \tag{45}$$

where $\overline{x}$, $\overline{y}$, $\overline{z}$ refer to a typical point (B) on the given extremal $\overline{C}$ and $\overline{x'}$, $\overline{y'}$, $\overline{z'}$ refer to the direction AB which is quite arbitrary. This is the Weiestrass necessary condition for a strong minimum. Assuming that V is continuous in all its six arguments, it follows that inequality (45) must hold for any neighboring curve C of arbitrary directions in a certain region surrounding $\overline{C}$. Hence this condition is also sufficient for a strong minimum. If, however, Eq. (45) holds only for small intervals of $\xi = \overline{x'} - \overline{x}$, $\eta = \overline{y'} - \overline{y}$, and $\mu = \overline{z'} - \overline{z}$, there is a weak minimum. In this case we may expand $\mathcal{E}$ in powers of ξ, η, and μ to obtain

$$\begin{aligned}\mathcal{E}(\overline{x'},\overline{y'},\overline{z'},\overline{x},\overline{y},\overline{z}) = \tfrac{1}{2}[&U_{\overline{x'}\overline{x'}}\xi^2 + (U_{\overline{x'}\overline{y'}} + U_{\overline{y'}\overline{x'}})\xi\eta + (U_{\overline{z'}\overline{y'}} \\ &+ U_{\overline{y'}\overline{z'}})\eta\mu + (U_{\overline{x'}\overline{z'}} + U_{\overline{z'}\overline{x'}})\xi\mu \\ &+ U_{\overline{y'}\overline{y'}}\eta^2 + U_{\overline{z'}\overline{z'}}\mu^2] + \cdots .\end{aligned} \tag{46}$$

Since this quadratic form should be positive for a minimum

$$U_{\overline{x'}\overline{x'}} > 0, \quad U_{\overline{x'}\overline{x'}}U_{\overline{y'}\overline{y'}} - U_{\overline{x'}\overline{y'}}U_{\overline{y'}\overline{x'}} > 0,$$

$$\begin{vmatrix} U_{\overline{x'}\overline{x'}} & U_{\overline{y'}\overline{x'}} & U_{\overline{z'}\overline{x'}} \\ U_{\overline{x'}\overline{y'}} & U_{\overline{y'}\overline{y'}} & U_{\overline{z'}\overline{y'}} \\ U_{\overline{x'}\overline{z'}} & U_{\overline{y'}\overline{z'}} & U_{\overline{z'}\overline{z'}} \end{vmatrix} > 0. \tag{47}$$

These are the Legendre's conditions (necessary and sufficient) for a weak minimum.

Because U is in general a complex quantity, we shall apply these criteria separately to characterize the extremals of the real and imaginary parts of U. Hence, from Eq. (47) the real and imaginary parts of $U_{x_i'x_j'}$ are to be real or, in other words, its complex phase has to belong to the interval $[0,\pi/2)$. Substitution of the constricted functional into expression (47) yields

$$U_{x_i'x_j'} = \frac{(\epsilon_{kk}\epsilon_{ij} - \epsilon_{ki}\epsilon_{kj})\dfrac{dx_i}{d\tau}\dfrac{dx_j}{d\tau}}{\left(\sqrt{\epsilon_{sm}\dfrac{dx_s}{d\tau}\dfrac{dx_m}{d\tau}}\right)^3}, \tag{48}$$

and thus, for a nematic liquid crystal for which $\epsilon_{ij} = \epsilon_\perp \delta_{ij} + \epsilon_a n_i n_j$, we have

$$\epsilon_{kk}\epsilon_{ij} - \epsilon_{ki}\epsilon_{kj} = (2\epsilon_\perp + \epsilon_\perp\epsilon_a)\delta_{ij} + \epsilon_\perp\epsilon_a n_i n_j . \tag{49}$$

Inserting this into Eq. (47) and taking the determinant, it leads to

$$\det(U_{x_i'x_j'}) = \frac{2\sqrt{\epsilon_\perp}(2\epsilon_\perp + \epsilon_a)}{(\epsilon_a + \epsilon_\perp)^{1/2}} > 0.$$

Therefore, to satisfy this inequality both the real and imaginary parts of $\epsilon_\perp$ should be positive, $\mathrm{Re}\epsilon_\perp \sim \mathrm{Im}\epsilon_\perp > 0$. This provides for a criterion that assures that the extremal is indeed a minimum.

VI. RESULTS

In the absence of absorption, the analytical expressions for the TM modes in terms of p or α for the different regions of the cell are given by Eqs. (20)–(22) in Ref. [19]. Note that the analytical solutions for $H_y^L(\zeta,k_0)$ and $H_y^R(\zeta,k_0)$ valid in the cladding and given by Eqs. (31) and (33), have the same form as in the case without absorption, but in the present case $\epsilon_\parallel$, $\epsilon_\perp$, ϵ_c, and p are complex quantities. With the purpose of evaluating the validity of our analytical results for the analytical propagation constants, β^{an} or p^{an}, and field amplitudes, $H_y^{an}(\zeta,k_0)$, obtained above in the WKB limit, in this section we calculate numerically the exact p^{num} and general solution, $H_y^{num}(\zeta,k_0)$, of Eqs. (31)–(33), and compare them with $H_y^{an}(\zeta,k_0)$.

To this end the analytical expressions for the amplitudes $H_y^L(\zeta,k_0)$ and $H_y^R(\zeta,k_0)$, Eqs. (31) and (32), for the isotropic cladding may be used as a starting point to calculate $H_y^{num}(\zeta,k_0)$ and $\partial H_y^{num}/\partial\zeta$ on the left interphase between cladding and nematic, by using the so called modified shooting method [35]. The basic idea is to use a Runge-Kutta routine to calculate these quantities on the right interphase by varying the real and imaginary parts of β, until $H_y^{num}(\zeta,k_0)$ and $\partial H_y^{num}/\partial\zeta$ take the values given by Eq. (30). This leads to a trascendental equation of the form

$$\begin{aligned}\Xi \equiv \Xi_r + i\Xi_i = &\frac{dH_y^{num}(\zeta = 0.5,p)}{d\zeta} \\ &+ k_0 l\sqrt{p^2 - \epsilon_c}H_y^{num}(\zeta = 0.5,p^{num}) = 0.\end{aligned} \tag{50}$$

Again, it should be emphasized that the solution $H_y^{num}(\zeta = 0.5,p^{num})$ and p^{num} are complex quantities. In Fig. 5 we plot the real, Ξ_r, and imaginary, Ξ_i, parts of Eq. (50) for the same range $(-0.001,0.001)$ used before and for $p = p^r + ip^i$ in the intervals $1 \leqslant p^r \leqslant 1.5$ and $0 \leqslant p^i \leqslant 0.3$, as shown in Fig. 4. The intersection of these curves yields the value of p^{num} corresponding to the lowest order mode, namely $(p_r^{num} = 1.404,\ p_i^{num} = 0.244)$, see inset in Fig. 5. Upon substitution of this complex eigenvalue p^{num} into the Runge-Kutta routine we get $\mathrm{Re}[H_y^{num}(\zeta,k_0)]$ and $\mathrm{Im}[H_y^{num}(\zeta,k_0)]$ plotted in Fig. 6 as functions of ζ.

Let us now compare the analytical results p^{an}, with the numerical ones p^{num}. If the relative error between the analytical and numerical calculations for p is measured by the ratio $\Lambda \equiv |p^{an} - p^{num}|/|p^{num}|$, from the above given values of these quantities we get $\Lambda = 9.92 \times 10^{-4}$, which amounts to a relative error of 0.1%. This shows that the analytical calculation of the propagation constants, $\beta = pk_0$, in the WKB

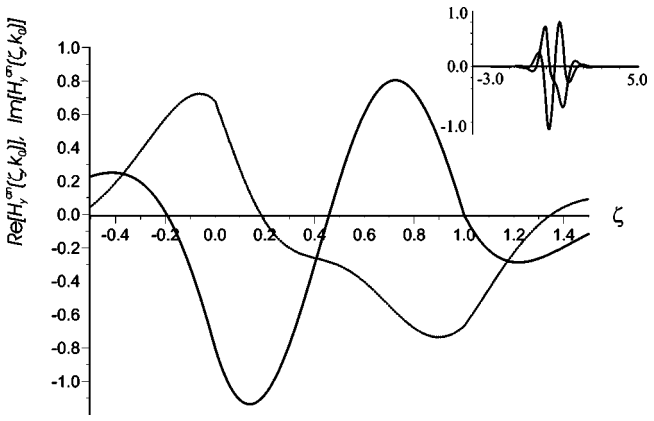

FIG. 5. Analytical real (—) and imaginary (- - -) parts of $H_y^{an}(\zeta,k_0)$ for the lowest order mode in the presence of absorption.

approximation is in excellent agreement with their numerical exact values. Thus, the WKB limit is a good approximation for these quantities.

If we now compare the real part of p, either analytical or numerical, $p^r=1.404$, with its magnitude in the absence of absorption calculated in Ref. [19], namely, $p^{wa}=1.35$, we get $p^{wa}/p^r\sim 4\%$. Thus, the effect of absorption on the propagation constant is small.

To compare the analytical and numerical estimates of the field amplitude $H_y(\zeta,t)$ in the presence of absorption, with its values when there is no absorption, we consider Figs. 7 and 6. These curves clearly show that these amplitudes are different in regard to the position of their maxima and minima, as well as in the magnitude of the discontinuities of $\partial H_y^{an}/\partial\zeta$ and $\partial H_y^{num}/\partial\zeta$ at the boundaries. Actually, these latter differences should be expected, since the WKB approximation only keeps up to second-order derivatives, while in the numerical calculation higher order derivatives are kept.

In order to quantify these differences in more detail, we first calculate the real, $\mathrm{Re}[H_y^{wa}(\zeta,k_0)]$, and imaginary parts, $\mathrm{Im}[H_y^{wa}(\zeta,k_0)]$, of the field amplitude in the case without absorption. Actually, this amplitude $H_y^{wa}(\zeta,k_0)$ and its phase

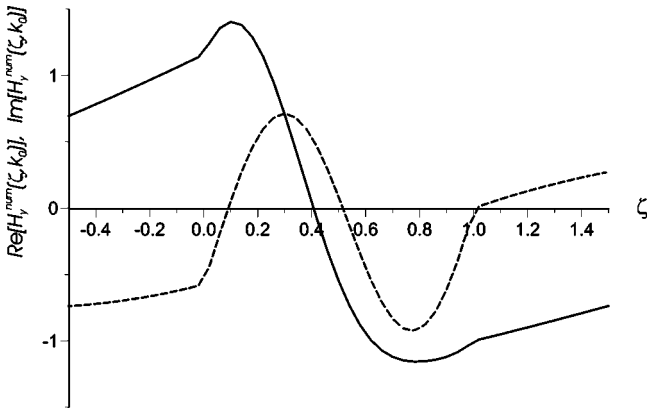

FIG. 6. Real (—) and imaginary (- - -) parts of the lowest order mode ($n=1$) $H_y^{num}(\zeta,k_0)$, as a function of ζ.

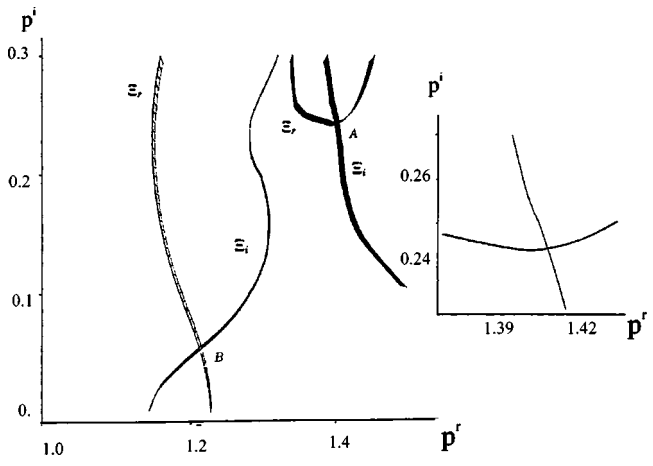

FIG. 7. Numerical solution of Eq. (1.4) for Ξ_r and Ξ_i in the range $(-0.001,0.001)$ and for the intervals $1\leqslant p^r\leqslant 1.5$ and $0\leqslant p^i\leqslant 0.3$. The inset shows in more detail solution A for the mode $n=1$.

were already calculated before in Ref. [19], Figs. 6(a) and 6(b), but they were not expressed in terms of the behavior of their real and imaginary parts. So, from Eqs. (20)–(22) in Ref. [19], we get the curves in Fig. 8. They show that before entering the cell both parts are in phase. Inside the cell the phase of the field decreases, so that its imaginary part tends to zero and vanishes at the edge of the cell at $\zeta=1$. Note that within the cell, $0\leqslant\zeta\leqslant 1$, the imaginary part $\mathrm{Im}[H_y(\zeta,k_0)]$ is much smaller than the real part $\mathrm{Re}[H_y(\zeta,k_0)]$. Also, a large part of $\mathrm{Re}[H_y(\zeta,k_0)]$ propagates to the cladding, so that a large portion of the field energy is not contained in the cell. The inset confirms this behavior and shows that it slowly vanishes in the cladding. It should be pointed out that in this case the imaginary part $\mathrm{Im}[H_y(\zeta,k_0)]$ arises from the anisotropy of the nematic and not from absorption effects, as shown explicitly in Eq. (11) in Ref. [19].

In contrast, our Fig. 7 shows that in the presence of absorption the real, $\mathrm{Re}[H_y^{an}(\zeta,k_0)]$, and imaginary,

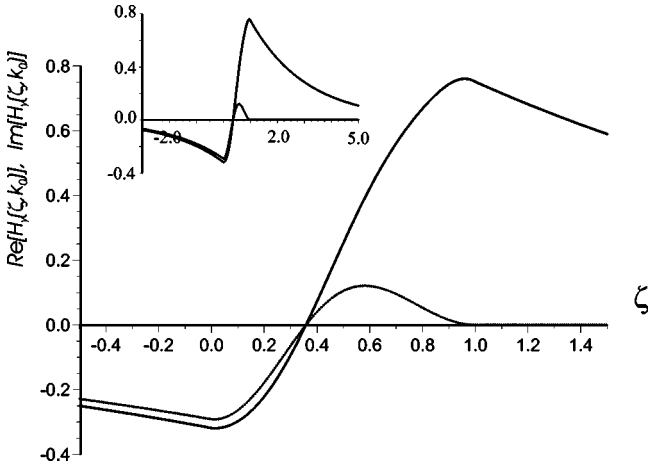

FIG. 8. Analytical real (—) and imaginary (- - -) parts of $H_y(\zeta,k_0)$ in the absorptionless case with $n=1$, as a function of ζ. Obtained from Eqs. (31)–(33) with real dielectric tensor components.

$\mathrm{Im}[H_y^{an}(\zeta,k_0)]$, parts, as calculated from Eqs. (31)–(33), are not in phase when they enter the cell because, as shown above, the propagation constant is imaginary in this case. Furthermore, their amplitudes are comparable at every point within the cell, showing that absorption is indeed a large effect. On the other hand, the energy propagated into the cladding is now much smaller than without absorption; in this sense, the presence of absorption confines the energy into the cell more efficiently, as confirmed by the curve in the inset in Fig. 7.

Consider now the amplitudes of the fields $H_y^{an}(\zeta,t)$ and $H_y^{num}(\zeta,t)$. Their differences may be quantified by calculating a sort of mean square error defined as

$$\Omega_r \equiv \int_{-\infty}^{\infty} [\mathrm{Re}(H_y^{num}) - \mathrm{Re}(H_y^{an})]^2 d\zeta, \tag{51}$$

$$\Omega_i \equiv \int_{-\infty}^{\infty} [\mathrm{Im}H_y^{num}) - \mathrm{Im}(H_y^{an})]^2 d\zeta, \tag{52}$$

where each term has been normalized to unity. From Figs. 7 and 6 we get $\Omega_r = 0.43$ and $\Omega_i = 0.59$. This result shows that in contrast to the difference found for the eigenvalues, the error between the numerical and the analytical calculation of the field amplitudes is larger. However, it should be stressed that both results have been derived on the basis of an analytical approach which indeed takes into account the effects due to absorption, but contains a restricting feature that is largely responsible for this result. Indeed, recall that choosing the value $k_0 l = 6.28$ does not strictly speaking corresponds to the WKB limit, defined by the condition $k_0 l \gg 1$. Although in the absorptionless case this value describes a waveguide with only two propagating modes, in the presence of absorption many solutions of Eq. (34) are possible, apart from the ones denoted by *A* and *B* in Fig. 4, implying the presence of many propagating modes. In spite of this, we have only considered two propagating modes because it simplifies considerably the solution of the complex trascendental equation (34). The consideration of a more suitable value of $k_0 l$ consistent with the WKB limit, makes the calculation of the graphic solution of Eq. (34) a formidable problem. In this sense we have carried out a first exploratory analytical calculation. Actually, similar differences between the field amplitudes were found in the case without absorption, when calculated from a pure numerical approach [20–22] and on the basis of an analytical approach [19,23].

VII. CONCLUDING REMARKS

Our model calculation shows, on the one hand, that absorption effects in the propagation of an optical field through a liquid crystal may in fact be accounted for by generalizing to lossy media a systematic formalism previously developed and whose first terms of its asymptotic expansion lead to the OL and the WKB limit. Our extension of Fermat's principle to consider media with complex dielectric tensor is discussed in Sec. V. It leads to complex ray trajectories whose real parts give the actual ray trajectory in the sense of phase wave, whereas the imaginary part gives the path of minimum absorption. When we compare the analytical or numerical calculation of the propagation constant with and without absorption, we get an excellent agreement, which indicates that for this property absorption effects are small. In contrast, a comparison of the field amplitudes for the absorption and absorptionless situations shows that absorption effects may be quite large and should be taken into account in the dynamic description.

The experiments reported in the literature where waveguide filled with dye-doped LC are involved [15,16] were realized at a wavelength range for which the absorption effect is small and performed for light intensities such that the nonlinear optical regime was developed. Thus, strictly speaking it is not correct to compare the system of the experiment of Ref. [15] with the one used in our calculation; however, we shall mention some ensuing similar qualitative features. Indeed, our results shown in Fig. 5 present an amplitude which contains the double of oscillations than those obtained for the first mode of an absorptionless waveguide (Fig. 8). In this sense the energy distribution seems to be split into two regions. Nevertheless, here the energy distribution is due to a larger magnitude of the wave vector caused by the imaginary part, which is not present in the absorptionless case; while for that of Ref. [15] it stems by a nonlinear reorientation after the occurrence of an optical Fredericks transition.

In conclusion, if these absorption effects could find some applications in fields like integrated nonlinear optics remains to be assessed.

ACKNOWLEDGMENTS

We are indebted to Professor P. Palffy-Muhoray for useful discussions and we acknowledge partial financial support under Grant No. DGAPA-UNAM IN101999 and from CONACYT Grant No. 41035, México.

[1] N.V. Tabiryan, A.V. Sukhov and Ya.B. Zeldovich, Mol. Cryst. Liq. Cryst. **136**, 1 (1986).
[2] I.C. Khoo and H. Li, Appl. Phys. B: Photophys. Laser Chem. **1**, 573 (1993).
[3] S.H. Chen and T.J. Chen, Appl. Phys. Lett. **64**, 1893 (1994).
[4] I.C. Khoo, L. Hong, P.G. LoPresti, and L. Yu, Opt. Lett. **19**, 530 (1994).
[5] I.C. Khoo, J. Nonlinear Opt. Phys. Mater. **8**, 305 (1999).
[6] J.A. Reyes and R.F. Rodríguez, J. Nonlinear Opt. Phys. Mater. **4**, 943 (1995).
[7] R.F. Rodríguez and J.A. Reyes, Mol. Cryst. Liq. Cryst. **282**, 287 (1996).
[8] J.A. Reyes and R.F. Rodríguez, Opt. Commun. **134**, 349 (1997).
[9] G. Hu, P. Palffy-Muhoray, and N. V. Tabiryan, *Licht-Und Teilchenoptik Annual Report* No. 47, 1993 (unpublished).
[10] T. Vogeler, N. V. Tabiryan, and M. Kreuzer, *Licht-Und Teilchenoptik Annual Report* No. 25, 1993 (unpublished).

[11] G. Abbate, F. Castaldo, L. De Stefano, E. Santamato, and P. Mormile, J. Phys. B **30**, 5587 (1997).
[12] I. Jánossy, J. Nonlinear Opt. Phys. Mater. **8**, 361 (1999).
[13] I. Jánossy, A.D. Lloyd, and B.S. Wherrett, Mol. Cryst. Liq. Cryst. **179**, 1 (1990).
[14] I. Jánossy and T. Kósa, Opt. Lett. **17**, 236 (1992).
[15] G. Abbate, L. de Stefano, E. Santamato, and G. Scalia, J. Nonlinear Opt. Phys. Mater. **8**, 319 (1999).
[16] L. Petti, L. De Stefano, P. Mormile, G.C. Righini, L. Sirleto, and G. Abbate, J. Opt. A, Pure Appl. Opt. **1**, 390 (1999).
[17] M.I. Barnik, A.S. Zolot'kov, and V.F. Kitaeva, JETP **84**, 1122 (1997).
[18] T. Kósa and I. Jánnosy, Opt. Lett. **20**, 1230 (1995).
[19] J.A. Reyes and R.F. Rodríguez, Mol. Cryst. Liq. Cryst. **317**, 135 (1998).
[20] H. Lin, D.S. Moroi, and P. Palffy-Muhoray, Mol. Cryst. Liq. Cryst. **223**, 241 (1992).
[21] H. Lin and P. Palffy-Muhoray, Opt. Lett. **17**, 722 (1992).
[22] H. Lin and P. Palffy-Muhoray, Opt. Lett. **19**, 436 (1994).
[23] J.A. Reyes and R.F. Rodríguez, Physica D **101**, 333 (2000).
[24] J.A. Reyes and R.F. Rodríguez, J. Nonlinear Opt. Phys. Mater. **6**, 81 (1997).
[25] D. Zwillinger, *Handbook of Differential Equations* (Academic Press, New York, 1989).
[26] H. Goldstein, *Classical Mechanics* (Addisson-Wesley, New York, 1986).
[27] G. Abate, P. Maddalena, L. Marrucci, and E. Santamato, Phys. Rev. E **52**, 5053 (1995).
[28] J. D. Marcuse, *Theory of Dielectric Optical Waveguides* (Academic Press, New York, 1974).
[29] J. D. Jackson, *Classical Electrodynamics* (Wiley, New York, 1975).
[30] M. Born and E. Wolf, *Principles of Optics* (Pergamon Press, New York, 1975).
[31] C. W. Misner, K. S. Throne, and J. A. Wheeler, *Gravitation* (Freeman, New York, 1973), Sec. 13.4.
[32] J.A. Reyes, J. Phys. A **32**, 3409 (1999).
[33] R. Lunemburg, *Mathemathical Theory of Optics* (University of California Press, Berkeley, 1964).
[34] L. E. Elsgoltz, *Differential Equations and the Calculus of Variations* (Mir, Moscow, 1970), Chap. 8.
[35] H. Williams *et al.*, *Numerical Recipes in Fortran: The Art of Scientific Computing*, 2nd ed. (Cambrige University Press, London, 1992).